Trans. Phenom. Nano Micro Scales, 6(Special):44-50
DOI: 10.22111/tpnms.2018.23937.1147

ORIGINAL RESEARCH PAPER

Numerical Investigating the Gas Slip Flow in the Microchannel Heat Sink Using Different Materials

Mojtaba Sepehrnia[1*], AhmadReza Rahmati[2]

[1]Department of Mechanical Engineering, Shahabdanesh University, Qom, Iran
[2]Department of Mechanical Engineering, University of Kashan, Kashan, Iran

Received 9 February 2018; accepted 10 March 2018; available online 6 May 2018

ABSTRACT: In this work, slip flow of helium gas has been studied in a three dimensional rectangular microchannel heat sink with 11 microchannel and 10 rectangular fins. Helium gas flow is considered ideal and incompressible. The finite volume method with using coupled algorithm is employed to carry out the computation. To validate the present work, comparison with numerical and experimental studies is done and it is seen that the computed results have good agreement. To investigate the effect of fins and walls material on heat sink performance, all simulations are carried out and compared with each other for three materials consisting of aluminum, silicon and copper. The results show that along the microchannel, local Knudsen number decreases. Also thermal resistance increases continuously with increasing Knudsen number from 0.006 to 0.048. The results indicate that for various inlet Knudsen numbers, copper heat sink has the lowest thermal resistance. Furthermore, copper heat sink has the highest average Nusselt number for Knudsen number higher than 0.024 but for Knudsen number lower than 0.024, silicon heat sink has higher average Nusselt number than copper heat sink.

KEYWORDS: *Heat sink; Ideal gas; Incompressible flow; Rectangular microchannel; Slip flow*

INTRODUCTION

In the recent decades, extensive researches have been done in context of micro and nano scale flows and its application in various industries such as electronic, medicine, aerospace, and so on. The concept of microchannel heat sink was firstly proposed by Tuckerman and Pease [1]. They analyzed a microchannel heat sink using water as the coolant. Zhu and Liao [2] investigated forced convective heat transfer for a gas flowing through a microchannel of arbitrary cross section with the axially-constant heat flux. They studied the slip flow and temperature jump regime using the orthonormal function method. Then, as a sample, they focused on investigating the heat transfer characteristics of rectangular and triangular microchannels. They indicated that the average Nusselt number in the slip flow regime is smaller than no slip flow regime. Hettiarachchi et al. [3] numerically studied heat transfer of gas flow in rectangular microchannel. With considering slip and temperature jump conditions for walls they showed that velocity slip increases the Nusselt number, while the temperature-jump tends to decrease it, and the combined effect could result in an increase or a decrease in the Nusselt number. Shojaeian and Dibaji [4] analyzed heat transfer through triangular microchannels over the slip flow regime. They showed that for constant aspect ratio, the values of Poiseuille number decrease with Knudsen number. They also showed that for low Reynolds number, the effect of Reynolds on the Nusselt number is considerable.

✉ *Corresponding Author Email: *m.sepehrnia@shahabdanesh.ac.ir*
Tel.: +982532317171; Note. This manuscript was submitted on *February* 9, 2018; published online *May* 6,2018.

Languri and Hooman [5] numerically investigated heat transfer of gas flow through a microchannel of semicircular cross-section. They considered temperature jump and slip velocity boundary conditions. They showed that unlike the fully developed flow that Nusselt number is independent of Reynolds and Prandtl numbers, for developing flow, it cannot be further generalized through microchannels. They also presented that the effect of slip velocity and temperature jump conditions on Nusselt number is dependent on the interaction of slip velocity and temperature jump. Shkarah et al. [6] studied laminar, developed, and steady state flow in a 3D microchannel. The used aluminum, silicon, and graphene as substrate materials. Their results showed that graphene most effectively decreases the thermal resistance. Izadi et al. [7] numerically studied laminar forced convection of a Al_2O_3–water nanofluid flowing in a micro heat sink. They showed that Nusselt number increases with volume fraction enhancement. Also they found that solid material has no effect on pressure drop increment. Mashaei et al. [8] investigated the effect of nanoparticles on laminar forced convection in a serpentine microchannel, numerically. They found that when the applied heat flux increases, the heat transfer rate increases and the pressure drop decreases. Also they showed that the best thermal-hydraulic performance occurs at the lowest Reynolds number and medium nanoparticle volume fraction. Shojaeian and Kosar [9], analytically, studied convective heat transfer and entropy generation on Newtonian and non-Newtonian fluid flows between parallel-plates. They applied slip boundary conditions and indicated that an increase in the slip coeffici-

Nomenclature

A	Cross section area
c_p	Specific heat
D_h	Hydraulic diameter of the channel
h	heat transfer coefficient
H	Height
k	Thermal conductivity
Kn	Knudsen number
L	Length
Nu	Nusselt number
P	Pressure
p	Wet perimeter
Po	Poiseuille number
Pr	Prandtl number
q	Heat flux
R_{th}	Themal resistance
T	Temperature
V	Fluid velocity
W	Width
x,y,z	Cartesian coordinates

Greek Symbols

γ	Specific heat ratio
λ	Molecular mean free path
μ	Dynamic viscosity
ρ	Density
σ_T	The thermal accommodation coefficient
σ_V	The momentum accommodation coefficient

Subscripts

ch	Channel
g	Gas
hs	Heat sink
in	Inlet
Local	Local
m	Mean
max	Maximum
out	Outlet
s	Solid
w	Wall

-ent leads to an increase in both Nusselt number and Bejan number, while it decreases entropy generation. Karimipour [10] studied heat transfer of nanofluid in a microchannel considering slip velocity and temperature jump by using lattice Boltzmann method. He showed that using nanofluid with lower slip coefficient and higher volume fraction and Pr has the highest heat transfer.

Khorasanizadeh and Sepehrnia [11] investigated water laminar flow in a trapezoidal microchannel heat sink with copper porous microchannels. They showed that using copper porous domain in heat sink is effective about 24.5% at cooling electronic chip.

Also, Khorasanizadeh and Sepehrnia [12] studied on performance of a silicon trapezoidal microchannel heat sink with various entry/exit configurations using variable properties. They assumed that conductivity of silicon is temperature-dependent. They showed that by assuming temperature-dependent conductivity of silicon, the heat transfer increases between 0.75% and 2.58%, the thermal resistance decreases between 1.15% and 4.97% and θ decreases between 2.41% and6.49%. In another research, Khorasanizadeh and Sepehrnia [13] investigated three dimensional numerical study on a trapezoidal microchannel heat sink with different inlet/outlet arrangements utilizing nanofluid. They showed A-type heat sink, for which the inlet and outlet are placed horizontally at the center of the north and the south walls, has a better heat transfer performance.

The most previous studies on heat transfer are related to liquid flow and slip condition is ignored, but in this paper slip flow of incompressible and ideal helium gas is studied. Also, in this paper, conjugate heat transfer in heat sink is considered and the material effect of slid part on heat transfer performance is studied.

GEOMETRIC CONFIGURATIONS

The geometric configuration of the microchannel heat sink is shown in Figure 1. Helium gas flow is entered from center of north wall and exited from center of south wall. Gas flow path is consisted of 5 parts which are: 1. Inlet. 2. Distributing area. 3. Microchannels. 4. Collecting area 5. Outlet.

Figure 2 shows a cross section of heat sink at z=9mm. As it is shown in Figure 2, the heat sink consists of 11 rectangular microchannels separated by 10 fins. The size of microchannels and fins is equal. Heat flux of 500 W/m^2 is applied at the bottom plate of heat sink that the electronic chip assumed directly attached to the base plate of the heat sink. All the surfaces of heat sink are assumed to be insulated. Helium gas is considered incompressible and ideal. The properties of fluid and solid are shown in Table. 1.

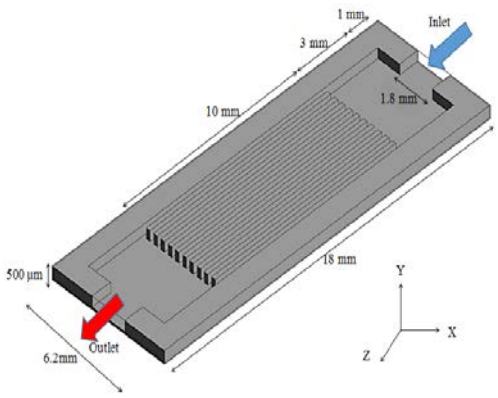

Fig. 1. Geometric configuration of micrchannel heat sink

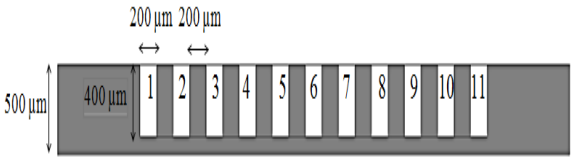

Fig. 2. Fin and microchannel dimensions (The created cross section at z=9mm)

Table 1
Properties of materials at 300 K [14].

Properties		Material
1.99E-5	μ (kg/ms)	Helium gas
5193	C_p (J/kg K)	
4.003	M (kg/kmol)	
0.152	k (W/m K)	
0.68	Pr	
1.667	γ	
0.073	σ_T	
0.9	σ_V	
Al: 237 Si: 148 Cu: 400	k (W/m K)	Solid

THE GOVERNING EQUATIONS AND BOUNDARY CONDITIONS

The continuity, momentum, and energy equations for a laminar, incompressible and steady state ideal gas flow can be written as follows:

$$\frac{\partial}{\partial x}(\rho u)+\frac{\partial}{\partial y}(\rho v)+\frac{\partial}{\partial z}(\rho w)=0 \tag{1}$$

$$\frac{\partial}{\partial x}(\rho uu)+\frac{\partial}{\partial y}(\rho vu)+\frac{\partial}{\partial z}(\rho wu)= -\frac{\partial p}{\partial x}+\frac{\partial}{\partial x}\left(\mu\frac{\partial u}{\partial x}\right)+\frac{\partial}{\partial y}\left(\mu\frac{\partial u}{\partial y}\right)+\frac{\partial}{\partial z}\left(\mu\frac{\partial u}{\partial z}\right) \tag{2}$$

$$\frac{\partial}{\partial x}(\rho uv)+\frac{\partial}{\partial y}(\rho vv)+\frac{\partial}{\partial z}(\rho wv)= -\frac{\partial p}{\partial y}+\frac{\partial}{\partial x}\left(\mu\frac{\partial v}{\partial x}\right)+\frac{\partial}{\partial y}\left(\mu\frac{\partial v}{\partial y}\right)+\frac{\partial}{\partial z}\left(\mu\frac{\partial v}{\partial z}\right) \tag{3}$$

$$\frac{\partial}{\partial x}(\rho uw)+\frac{\partial}{\partial y}(\rho vw)+\frac{\partial}{\partial z}(\rho ww)= -\frac{\partial p}{\partial z}+\frac{\partial}{\partial x}\left(\mu\frac{\partial w}{\partial x}\right)+\frac{\partial}{\partial y}\left(\mu\frac{\partial w}{\partial y}\right)+\frac{\partial}{\partial z}\left(\mu\frac{\partial w}{\partial z}\right) \tag{4}$$

$$\frac{\partial}{\partial x}(\rho uT)+\frac{\partial}{\partial y}(\rho vT)+\frac{\partial}{\partial z}(\rho wT)= \frac{\partial}{\partial x}\left(\frac{k}{c_p}\frac{\partial T}{\partial x}\right)+\frac{\partial}{\partial y}\left(\frac{k}{c_p}\frac{\partial T}{\partial y}\right)+\frac{\partial}{\partial z}\left(\frac{k}{c_p}\frac{\partial T}{\partial z}\right) \tag{5}$$

$$\frac{\partial}{\partial x}\left(k_s\frac{\partial T}{\partial x}\right)+\frac{\partial}{\partial y}\left(k_s\frac{\partial T}{\partial y}\right)+\frac{\partial}{\partial z}\left(k_s\frac{\partial T}{\partial z}\right)=0 \tag{6}$$

The boundary conditions for governing equations are dependent on operating conditions of the heat sink. In industrial applications, heat sink is attached to a heat generation source such as electronic chip. Helium gas flow is entered to heat sink with initial temperature and pressure.

The boundary conditions are related to the heat sink operational conditions. In practical applications, to receive heat and dissipate it by the fluid flow, heat sink is attached to a heat generation source such as an electronic chip. In this study, similar to the study of Li et al. [15], the pressure drop is adopted a constant.

According to operating conditions explained above, the boundary conditions for the governing equations are:
Inlet:

$$P=P_{\text{in}},\quad T=T_{\text{in}}=300K \tag{7}$$

Outlet:

$$P=P_{\text{out}}=200\,\text{Pa}=\text{Cte},\quad \frac{\partial T}{\partial n}=0 \tag{8}$$

At the base plate:

$$q_{\text{w}}=-k_{\text{s}}\frac{\partial T_{\text{s}}}{\partial n} \tag{9}$$

P_{in} and T_{in} are the helium gas inlet pressure and temperature, respectively, *p*out is the pressure at the outlet, *n* is the direction normal to the wall, and q_w is the heat flux applied at the base plate of the heat sink.

Slip velocity boundary condition at gas-solid interface for walls in Y-Z plane is:

$$w_{\text{w}}-w_{\text{g}}=\left(\frac{2-\sigma_v}{\sigma_v}\right)\text{Kn}\,L_c\left(\frac{\partial w}{\partial n}\right)\approx\left(\frac{2-\sigma_v}{\sigma_v}\right)\frac{\lambda}{\delta}(w_{\text{g}}-w_c) \tag{10}$$

$$u_{\text{g}}\equiv(\vec{u}.\vec{\text{n}})_{\text{g}}=u_w \tag{11}$$

In equation10, w and u represent the velocity components that are parallel and normal to the wall, respectively.

σ_y , $w_{c,}$, L_c and δ are the momentum accommodation coefficient, the velocity parallel to the wall, characteristic length and the distance from cell center to the wall respectively.

The temperature jump boundary condition at the gas-solid interface for walls in Y-Z plane is:

$$T_{\text{w}}-T_{\text{g}}=\left(\frac{2-\sigma_T}{\sigma_T}\right)\text{Kn}\,L_c\left(\frac{\partial T}{\partial n}\right)\approx 2\left(\frac{2-\sigma_T}{\sigma_T}\right)\frac{\lambda}{\delta}(\text{T}_{\text{g}}-T_c) \tag{12}$$

In equation 12, σ_T is the thermal accommodation coefficient.

In order to achieve dimensionless slip velocities in directions of X, Y, and Z, following equations are used:

$$u^* = \frac{u_{\text{slip}}}{u_{\text{slip,m}}} \tag{13}$$

$$v^* = \frac{v_{\text{slip}}}{v_{\text{slip,m}}} \tag{14}$$

$$w^* = \frac{w_{\text{slip}}}{w_{\text{slip,m}}} \tag{15}$$

The index m shows average velocity of gas. The dimensionless Poiseuille number can be calculated following equation:

$$Po = \frac{\Delta P D_h^2}{2L_{hs}\mu V_{\text{m,fluid}}^2} = \text{f} \times \text{Re} \tag{16}$$

The local dimensionless Poiseuille number is defined as follow:

$$Po_{\text{local}} = \frac{(P_{\text{local}} - P_{\text{out}})D_{\text{h}}^2}{2L_{\text{hs}}\mu V_{\text{m,local}}^2} \tag{17}$$

To investigate performance of heat sink, average Nusselt number and thermal resistance are defined as:

$$Nu_{\text{m}} = \frac{hD_{\text{h}}}{k_{\text{g}}} \tag{18}$$

h is the average convection heat transfer coefficient and can be calculated following equation

$$q_{\text{w}} = h\left(T_{\text{hs, m}} - T_{\text{g, m}}\right) \tag{19}$$

Where $T_{\text{hs,m}}$ and $T_{\text{g,m}}$ are the overall averaged temperatures of both heat sink and helium gas, respectively

$$Nu_{\text{m}} = \frac{q_{\text{w}}D_{\text{h}}}{k_{\text{g}}\left(T_{\text{hs, m}} - T_{\text{g, m}}\right)} \tag{20}$$

D_{h} is hydraulic diameter of the rectangular microchannel and obtained as:

$$D_{\text{h}} = \frac{4A}{p} \tag{21}$$

A is microchannel cross section area and p is wet perimeter.

The thermal resistance is obtained from the following equation:

$$R_{\text{th}} = \frac{T_{\text{w,max}} - T_{\text{in}}}{q_{\text{w}}W_{\text{hs}}L_{\text{hs}}} \tag{22}$$

In equation 22, $T_{\text{w,max}}$ is maximum temperature of the heat sink base plate.

NUMERICAL PROCEDURE, VALIDATION AND GRID INDEPENDENCY ANALYSIS

It should be noted that the convergence criterion in all runs was set at 10^{-10}. The computational method used in the present work was validated by comparing the simulation results with those of Chein and Chen [16] for the same geometry and simulation conditions and are compared in Table 2.

The relative difference of average Nusselt between present work and Chein and Chen [16] is lower than 2.6 that indicate a good validation of simulations.

Also in Figure 3 the local Nusselt number values along the microchannel #5 have been compared with those of Philips [17] for the pressure drop of 50 kPa. The trend of local Nusselt number change along microchannel #5 is the same as that of Philips[17].

Table 2
Comparisons between the average Nusselt number results with Chein and Chen [16].

Pressure drop(kPa)	Present study	Chein and Chen[16]	Relative difference(%)
25	8.35	8.45	1.1
35	9.01	9.13	1.3
50	9.64	9.9	2.6

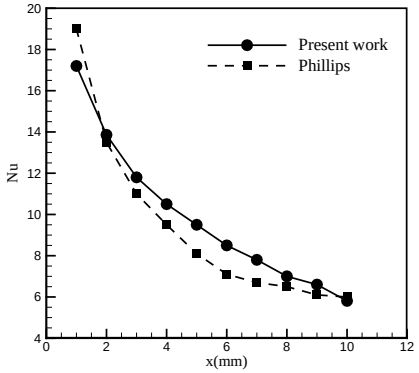

Fig. 3. Variation of local Nusselt number along microchannel #5 for the the experimental study of Phillips [17] at $\Delta P = 50$ kPa

Preliminary tests were carried out to test the accuracy of the numerical solution.

To this scope seven different grids were compared in terms of temperature.

The values of temperature and number of elements are reported in Figure 4.

In Figure 4, the variation of local temperature for helium gas flow is presented at pressure ratio of 8 and heat flux of 500 W/m^2 in center of the sixth aluminum microchannel heat sink.

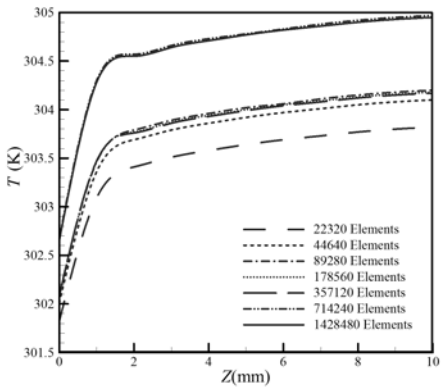

Fig.4. Variation of temperature for helium gas flow at pressure ratio of 8 and heat flux of 500 W/m^2

RESULTS AND DISCUSSION

The simulations have been performed for slip flow of helium gas in a three dimensional rectangular microchannel heat sink with 11 microchannel and 10 rectangular fins. Helium gas flow has been considered ideal and incompressible. The finite volume method with using coupled algorithm has been employed to carry out the computation. In the following the results of this study are presented and discussed.

In Figure 5, the variation of inlet Knudsen number in terms of inlet to outlet pressure ratio has been shown for aluminum heat sink. As it is observed from Figure 5, inlet Knudsen number decreases with increasing pressure ratio because with increasing pressure ratio, density of gas increases and with increasing density, the molecular mean free path and subsequently Knudsen number decreases.

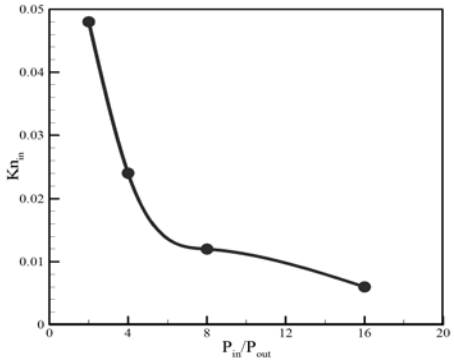

Fig.5. The variations of Knudsen number in terms of inlet to outlet pressure ratio

The variations of local Poiseuille number along the sixth microchannel are shown in Figure 6 for aluminum microchannel. With decreasing Knudsen number, local Poiseuille number increases. Because the pressure outlet is constant, according to equation 20, with increasing pressure inlet, local pressure and velocity enhances. Increasing or decreasing Poiseuille number is dependent on the interaction of variation of this two local parameter, velocity and pressure, and overcome one of them over another because other parameters of equation 17 are constant. Therefore, when inlet pressure increases, increasing local pressure relative to increasing local average velocity is dominant at each section of the microchannel. So, Poiseuille number increases at each pint.

In Figure 7, the variations of local Knudsen number in terms of various pressure ratios are shown along the sixth microchannel for aluminum heat sink. In the flow direction, pressure decreases because of gas flow friction with walls; therefore, the molecular mean free path and subsequently local Knudsen number increase.

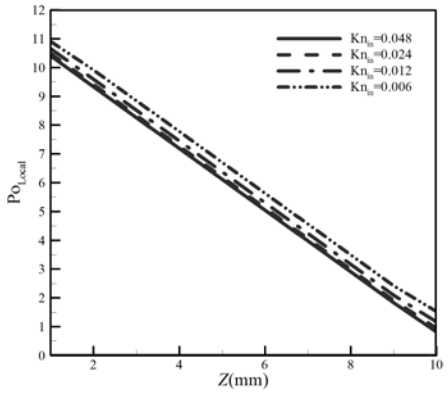

Fig.6. The variations of Poiseuille number along the sixth microchannel

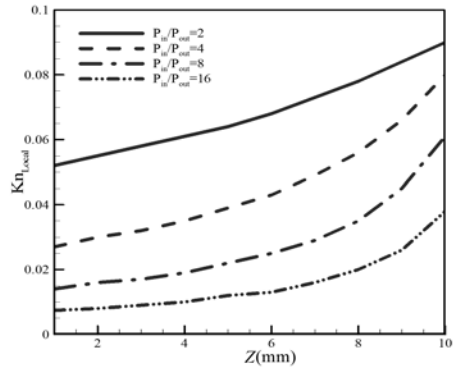

Fig.7. The variations of local Knudsen number along the sixth microchannel

In Figure 8, the variations of average Nusselt number in terms of Knudsen number is indicated for three types of heat sink. As it is obvious, with increasing Knudsen number, first, average Nusselt number drcreases and then increases. Table 3 indicate average gas temperature, average heat sink temperature, and difference between these two temperatures for various inlet pressure is used to proper analysis of the changes of average Nusselt number in terms of Knudsen number. As, it is obvious from Table 3, with decreasing Knudsen number and increasing pressure, heat transfer increases and average temperature of heat sink decreases. Also, with decreasing Knudsen number and increasing pressure, gas velocity enhances so sufficient opportunity to

heat transfer to upper layers of gas decreases. Therefore, the average temperature of gas decreases.

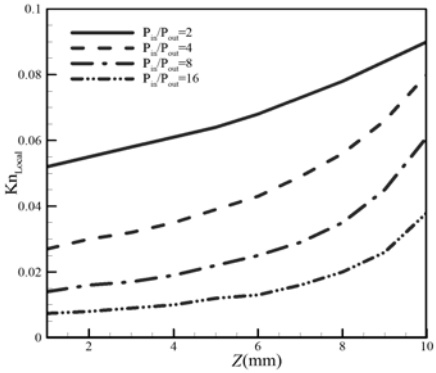

Fig.8. The varations of Nusselt number in terms of Knudsen number for three types of heat sink and heat flux of 500W/m^2

Table 3
The average temperature of gas and heat sink in terms of inlet Knudsen number for heat flux of 500 W/m^2.

Inlet Knudsen number	Average temperature of gas (K)	Average Temperature of heat sink (K)	Difference Temperature of gas and heat sink(K)
0.006	301.988	302.321	0.333
0.012	304.242	304.773	0.531
0.024	309.949	310.678	0.729
0.048	326.521	327.212	0.691

Table 4
The variations of thermal resistance in terms of Knudsen number for three type of heat sink and heat flux of 500 W/m^2.

Inlet Knudsen number	Copper	Silicon	Aluminum
0.006	45.899	46.963	46.349
0.012	90.615	91.541	91.005
0.024	196.837	198.381	197.485
0.048	491.627	498.029	494.255

According to equation 20, the difference between the two these temperature shown in Table 3 is significant to calculate Nusselt number. As it can be seen, with increasing Knudsen number from 0.006 to 0.024, temperature difference between gas and heat sink increases. According to equation 20, average Nusselt number decreases. Temperature difference between gas and heat sink decreases with increasing Knudsen number from 0.024 to 0.048 that lead to increasing average Nusselt number. Quantitative studies show that with increasing inlet Knudsen number from 0.006 to .024, average Nusselt number decreases about 54.4% and with increasing inlet Knudsen number from 0.024 to 0.048, average Nusselt number increases about 5.42%. The results show that at Knudsen number of 0.024, three types of heat sink have approximately the same average Nusselt number. For Knudsen numbers lower than 0.024 silicon heat sinks and for Knudsen numbers higher than 0.024 copper heat sinks are more efficient.

The variation of thermal resistance in terms of Knudsen number is presented in Table 4 for three types of heat sink and heat flux of 500W/m^2. As it is seen, thermal resistance increases with increasing Knudsen number because with increasing Knudsen number, pressure flow and gas velocity decrease except at walls. Convection heat transfer decreases with decreasing gas velocity, so the maximum temperature of solid part of heat sink enhances. Due to increasing the maximum temperature of heat sink, according to equation 22, thermal resistance increases. Studies show that with increasing inlet Knudsen number from 0.006 to 0.048, thermal resistance enhances 966.34 percent.

CONCLUSIONS

Numerical analysis for ideal helium gas flow was performed in the range of Knudsen number 0.006<Kn<0.048. Constant heat flux of 500 W/m^2 was applied at the base plate of the heat sink. The material of heat sink and fins was considered aluminum. The following conclusions can be made based on the simulated results:

1- With increasing pressure ratio, Knudsen number decreases and Poiseuille number increases. In other words, slip rate decreases and friction rate increases.
2- Knudsen number increases along the microchannel because of decreasing helium gas pressure.
3- With enhancing Knudsen numer from 0.006 to 0.048, thermal resistance increases.
4- For all heat sinks studied, with increasing inlet Knudsen number from 0.006 to 0.024, the average Nusselt number decreases and with increasing Knudsen number from 0.024 to 0.48, the average Nusselt number increases.
5- The copper microchannel heat sink, for all inlet Knudsen number, has the lowest thermal resistance. Also, it has the highest average Nusselt number for inlet Knudsen number higher than 0.024.

REFERENCES

[1] Tuckerman DB, Pease R. High-performance heat sinking for VLSI. Electron Device Letters, IEEE. 1981;2(5):126-9.
[2] Zhu X, Liao Q. Heat transfer for laminar slip flow in a microchannel of arbitrary cross section with complex thermal boundary conditions. Applied Thermal Engineering. 2006;26(11-12):1246-56.
[3] Hettiarachchi HM, Golubovic M, Worek WM, Minkowycz W. Three-dimensional laminar slip-flow and heat transfer in a rectangular microchannel with constant wall temperature. International Journal of Heat and Mass Transfer. 2008;51(21-22):5088-96.
[4] Shojaeian M, Dibaji SAR. Three-dimensional numerical simulation of the slip flow through triangular microchannels. International Communications in Heat and Mass Transfer. 2010;37(3):324-9.

[5] Languri EM, Hooman K. Slip flow forced convection in a microchannel with semi-circular cross-section. International Communications in Heat and Mass Transfer. 2011;38(2):139-43.

[6] Shkarah AJ, Sulaiman MYB, Ayob MRBH, Togun H. A 3D numerical study of heat transfer in a single-phase micro-channel heat sink using graphene, aluminum and silicon as substrates. International Communications in Heat and Mass Transfer. 2013;48:108-15.

[7] Izadi M, Shahmardan M, Rashidi A. Study on Thermal and Hydrodynamic Indexes of a Nanofluid Flow in a Micro Heat Sink. Transport Phenomena in Nano and Micro Scales. 2013;1(1):53-63.

[8] Rahim Mashaei P, Hosseinalipour S, El Jawad Muslmani M. The Impact of Nanoparticles on Forced Convection in a Serpentine Microchannel. Transport Phenomena in Nano and Micro Scales. 2014;2(2):86-99.

[9] Shojaeian M, Koşar A. Convective heat transfer and entropy generation analysis on Newtonian and non-Newtonian fluid flows between parallel-plates under slip boundary conditions. International Journal of Heat and Mass Transfer. 2014;70:664-73.

[10] Karimipour A. New correlation for Nusselt number of nanofluid with $Ag/Al_2O_3/Cu$ nanoparticles in a microchannel considering slip velocity and temperature jump by using lattice Boltzmann method. International Journal of Thermal Sciences. 2015;91:146-56.

[11] Khorasanizadeh H, Sepehrnia M. Effects of different inlet/outlet arrangements on performance of a trapezoidal porous microchannel heat sink. 2016.

[12] Khorasanizadeh H, Sepehrnia M. Performance Evaluation of a Trapezoidal Microchannel Heat Sink with Various Entry/Exit Configurations Utilizing Variable Properties. Journal of Applied Fluid Mechanics. 2017;10(6):1547-59.

[13] Khorasanizadeh H, Sepehrnia M. Three dimensional numerical study on a trapezoidal microchannel heat sink with different inlet/outlet arrangements utilizing variable properties nanofluid. Transport Phenomena in Nano and Micro Scales. 2018(Accepted).

[14] Bergman TL, Incropera FP. Fundamentals of heat and mass transfer: John Wiley & Sons; 2011.

[15] Li J, Peterson G, Cheng P. Three-dimensional analysis of heat transfer in a micro-heat sink with single phase flow. International Journal of Heat and Mass Transfer. 2004;47(19):4215-31.

[16] Chein R, Chen J. Numerical study of the inlet/outlet arrangement effect on microchannel heat sink performance. International Journal of Thermal Sciences. 2009;48(8):1627-38.

[17] Phillips RJ. Microchannel Heat Sinks. Lincoln Laboratory Journal. 1988;1(1).